

Article

Not peer-reviewed version

Tailoring Photoluminescence and X-ray Storage Properties in Mechanochemically Prepared Nanocrystalline $\text{CaF}_2:\text{Sm}^{3+}$

[Z. Siti Rozaila](#) , [Nicolas Riesen](#) , [Hans Riesen](#) *

Posted Date: 29 November 2024

doi: 10.20944/preprints202411.2369.v1

Keywords: ball milling; dopant concentration; post-annealing treatment; calcium fluoride; samarium; mechanochemistry; storage phosphors; solid state chemistry



Preprints.org is a free multidisciplinary platform providing preprint service that is dedicated to making early versions of research outputs permanently available and citable. Preprints posted at Preprints.org appear in Web of Science, Crossref, Google Scholar, Scilit, Europe PMC.

Copyright: This open access article is published under a Creative Commons CC BY 4.0 license, which permit the free download, distribution, and reuse, provided that the author and preprint are cited in any reuse.

Article

Tailoring Photoluminescence and X-Ray Storage Properties in Mechanochemically Prepared Nanocrystalline $\text{CaF}_2:\text{Sm}^{3+}$

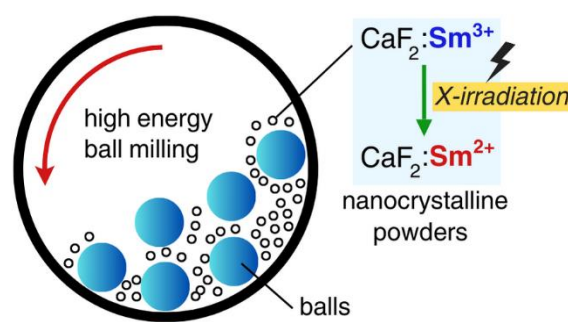
Z. Siti Rozaila ¹, Nicolas Riesen ² and Hans Riesen ^{1,*}

¹ School of Science, The University of New South Wales, Canberra, ACT 2600, Australia.

² ARC Research Hub for Integrated Devices for End-user Analysis at Low-Levels (IDEAL), Future Industries Institute, STEM, University of South Australia, Mawson Lakes, SA 5095, Australia.

* Correspondence: h.riesen@adfa.edu.au; Hans Riesen – School of Science, The University of New South Wales, Canberra, ACT 2600, Australia; orcid.org/0000-0002-3386-6551; Email: h.riesen@adfa.edu.au

TOC Graphic



Abstract: The mechanochemical preparation of nanocrystalline $\text{CaF}_2:\text{Sm}^{3+}$ by ball milling calcium acetate hydrate, samarium (III) acetate hydrate, and ammonium fluoride is reported. The photoluminescence of the as-prepared $\text{CaF}_2:\text{Sm}^{3+}$ shows predominantly $\text{Sm}^{3+} {}^4\text{G}_{5/2} \rightarrow {}^6\text{H}_j$ ($J = 5/2, 7/2, 9/2$, and $11/2$) f-f luminescence, but electric dipole allowed $4f^5 5d ({}^1\text{T}_{1u}) \rightarrow 4f^6 {}^7\text{F}_1 ({}^1\text{T}_{1g})$ luminescence by Sm^{2+} was generated upon X-irradiation. In comparison with the co-precipitated $\text{CaF}_2:\text{Sm}^{3+}$, the conversion of $\text{Sm}^{3+} \rightarrow \text{Sm}^{2+}$ in the ball milling-sample upon X-irradiation is significantly lower. Importantly, the present results indicate that the crystallite size and X-ray storage phosphor properties of the lanthanide-doped nanocrystalline CaF_2 can be modified by adjusting the ball milling time, dopant concentration, and post-annealing treatment, and crystallite sizes as low as 6 nm resulted under specific experimental conditions.

Keywords: ball milling; dopant concentration; post-annealing treatment; calcium fluoride; samarium

1. Introduction

CaF_2 belongs to the alkaline earth metal fluoride (MF_2) compounds which crystallize in the cubic structure with the $Fm\bar{3}m$ space group.[1,2] The Ca^{2+} ions lie at the nodes in the face-centered lattice, while the F lie at the center of the octants.[3,4] There has been growing interest in studying the optical properties of lanthanide (Ln) doped CaF_2 due to the high transmittance from the far UV to the mid IR range, high chemical resistance, and low refractive index of this host.[5]

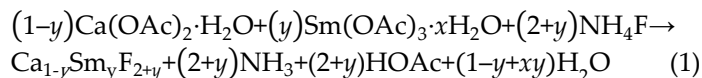
Nanocrystalline $\text{CaF}_2:\text{Ln}$ has been prepared by a wide variety of methods such as co-precipitation,[6,7] sol-gel process,[8] hydrothermal synthesis,[9,10] and thermal decomposition of precursors.[11] In recent years, high-energy ball milling has increasingly been applied to synthesize

stoichiometric and non-stoichiometric solid solutions with minimal or solvent free routes.[12–15] In this process, the mechanical energy caused by the high speed collision of balls in the ball milling jar forces the reagents to react and turn into fine powders that can be on the nanoscale.[16] This method has advantages in increasing the material reactivity, uniform spatial distribution of elements, and reducing the possibility of multi-phase formation.[17,18] Heise *et al.*[19] successfully synthesized Eu³⁺ doped MF₂ (M = Ca, Sr, and Ba) powders by ball milling M(OAc)₂, Eu(OAc)₃, and NH₄F, and crystallite sizes in the range of 12 to 18 nm were obtained. Molaiyan and Witter also reported the preparation of the CaF₂:Sm³⁺ electrolyte by ball milling anhydrous CaF₂ and SmF₃ in stoichiometric compositions of Sm_{1-y}Ca_yF_{3-y} (0 ≤ y ≤ 0.15) using a Tanchen planetary ball mill.[14] Although ball milling is a facile method in preparing nanocrystalline powders, this method has still not been widely applied to the preparation of MF₂:Ln materials for optical applications.

We have previously reported that nanocrystalline CaF₂:Sm³⁺ prepared by a co-precipitation method can serve as a relatively efficient photoluminescent X-ray storage phosphor, with the storage mechanism based on the reduction of Sm³⁺ to Sm²⁺ upon exposure to X-irradiation.[20] In the present study, we report the mechanochemical synthesis of nanocrystalline CaF₂:Sm³⁺ by ball milling Ca(OAc)₂, Sm(OAc)₃, and NH₄F at room temperature. The synthesized powders were characterized by XRD, electron microscopy, and luminescence spectroscopy. The effects of the ball milling time, Sm concentration, and post-annealing on the generation of Sm²⁺ by X-ray was investigated in detail using photoluminescence measurements.

2. Experimental Methods

Nanocrystalline CaF₂:ySm³⁺ (y = mol%) was prepared by ball milling Ca(OAc)₂·H₂O (May & Baker Ltd), Sm(OAc)₃·xH₂O (Sigma Aldrich), and NH₄F (Sigma Aldrich) according to the following solid-state reaction:



Reagents (with y = 0.1%) were premixed and ground using a mortar and pestle before being transferred into a 12 ml zirconia ball mill jar with six 5 mm diameter zirconia balls. The mixtures were then ball milled for 1, 3, 5 or 8 h to investigate the dependence of physical properties on ball milling time. The ball milling was performed using a Fritsch Planetary Mill (Pulverisette 7) at 10 Hz. The obtained mixture was dried overnight in an oven (Labec, Model H323) at 60 °C. The final product was then ground using a mortar and pestle to yield a homogenous nanocrystalline powder. Nanocrystalline CaF₂:ySm³⁺ powders with different Sm concentrations (y = 0, 0.05, 0.1, 0.3, 0.5, 1, 3, and 5 %) were also prepared with a ball milling time of 8 h. Post-annealing by using a muffle furnace (Labec, CEMLS-SD) was conducted at temperatures of 200, 300, and 400 °C in air.

The phase purity of samples was characterized by powder X-ray diffraction (XRD) on a Rigaku MiniFlex-600 benchtop diffractometer with Cu-Kα radiation (λ = 0.154 nm, 40 kV and 15 mA) with a scanning step and speed of 0.01° and 0.5°/min, respectively. Data was collected in the 2θ range of 10 to 100°. TEM imaging was undertaken by a FEI Tecnai G2 Spirit transmission electron microscope.

Photoluminescence (PL) spectra of Sm³⁺ were measured by using a Horiba Jobin-Yvon Spex FluoroMax-3 fluorometer at room temperature with 405 nm excitation. Sm²⁺ luminescence spectra were recorded on a Spex 500 M monochromator (150 grooves/mm grating), equipped with an Andor iDus camera (DV401A-BV Si CCD). A closed-cycle cryostat (CTI-Cryogenics Cryodyne model 22) was used to cool the sample to 27 K. In this case, the samples were excited by a focused 635 nm laser diode. The powders were manually pressed into a counterbore of 5 mm diameter and 0.5 mm depth on an aluminium holder.

The X-ray based reduction of Sm³⁺ to Sm²⁺ was undertaken on the Rigaku Miniflex-600 benchtop powder XRD diffractometer at a 2θ angle of 30° (dose rate ~15 mGy s⁻¹). The X-ray dose was cross-calibrated against a Sirona HELIODENT Plus dental X-ray source.

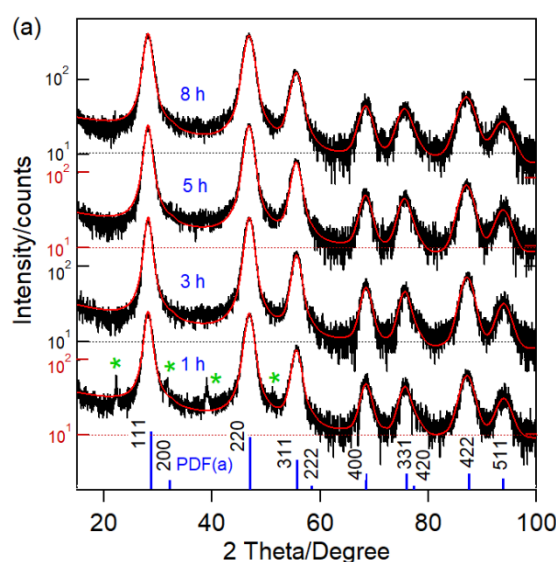
3. Results and Discussions

The XRD patterns of nanocrystalline $\text{CaF}_2:0.1\%\text{Sm}^{3+}$ prepared by ball milling with periods of 1, 3, 5 and 8 h are shown in Figure 1a. In Figure 1b the XRD patterns of $\text{CaF}_2:y\text{Sm}^{3+}$ ball milled for 8 h with different concentrations of Sm^{3+} ($0 \leq y \leq 5\%$) are illustrated. Finally, in Figure 1c the XRD patterns of $\text{CaF}_2:0.1\%\text{Sm}^{3+}$ (8 h ball milling period) annealed at temperatures of 200, 300, and 400 °C are shown. The patterns were compared with the standard CaF_2 data (PDF-1000043) taken from the Crystallography Open Database.[21] Results from Rietveld refinements obtained by the MAUD[22] software package are summarized in Table 1. The goodness of fit $G = R_{wp}/R_{exp}$ is < 1.5 for all refinements, i.e. implying good fits.[23] As follows from the figures, all the prominent peaks could be indexed to the cubic CaF_2 structure with the $Fm\bar{3}m$ space group.[1,2]

As seen in Figure 1a, impurity peaks are still visible after 1 h of milling. A more complete phase formation of nanocrystalline CaF_2 can be observed after 3 h. Importantly, prolonged ball milling broadened the diffractions peaks, and this was caused by the decrease of the average crystallite size of $\text{CaF}_2:0.1\%\text{Sm}^{3+}$ from 12 ± 1 to 8 ± 1 nm for ball milling times of 1 to 8 h (Table 1a). A 0.14% expansion of the lattice parameter was also observed with this decrease in the crystallite size. It is noted here that the use of hydrated salts in ball milling may accelerate the formation of $\text{CaF}_2:y\text{Sm}^{3+}$ due to the higher mobility of ions and this was also observed in the preparation of nanocrystalline BaFCl . [24]

Interestingly, a reduction of the average crystallite size of $\text{CaF}_2:y\text{Sm}^{3+}$ from 12 ± 1 to 6 ± 1 nm (Table 1b) was observed when the Sm^{3+} concentration was increased from 0 to 5 %. The lattice parameter also increased by 0.17 % in this case. The latter is most likely caused by the mechanism of charge compensation as Sm^{3+} substitutes Ca^{2+} . The excess positive charge must be compensated by defects such as O^{2-} impurity ions, substituting F^- in the lattice, and/or interstitial F^- . Also, the electronic repulsion of the ions may increase the lattice parameter. [25,26] Importantly, Sm^{3+} can easily substitute Ca^{2+} in the O_h symmetry with eightfold (bcc) coordination, due to their similar ionic radii ($\text{Sm}^{3+} = 1.08 \text{ \AA}$, compared to $\text{Ca}^{2+} = 1.12 \text{ \AA}$) [27] and, importantly, phase purity is retained for Sm^{3+} concentrations up to 5%.

As follows from Figure 1c, the annealing of $\text{CaF}_2:0.1\% \text{Sm}^{3+}$ at 200, 300, and 400 °C significantly narrowed the diffraction peaks. From the Rietveld refinements average crystallite sizes of 12, 22, and 46 ± 1 nm, respectively, were obtained for these annealing temperatures (Table 1c). The crystallite size appeared to grow by $\sim T^{3.4}$ upon annealing up to 400 °C.



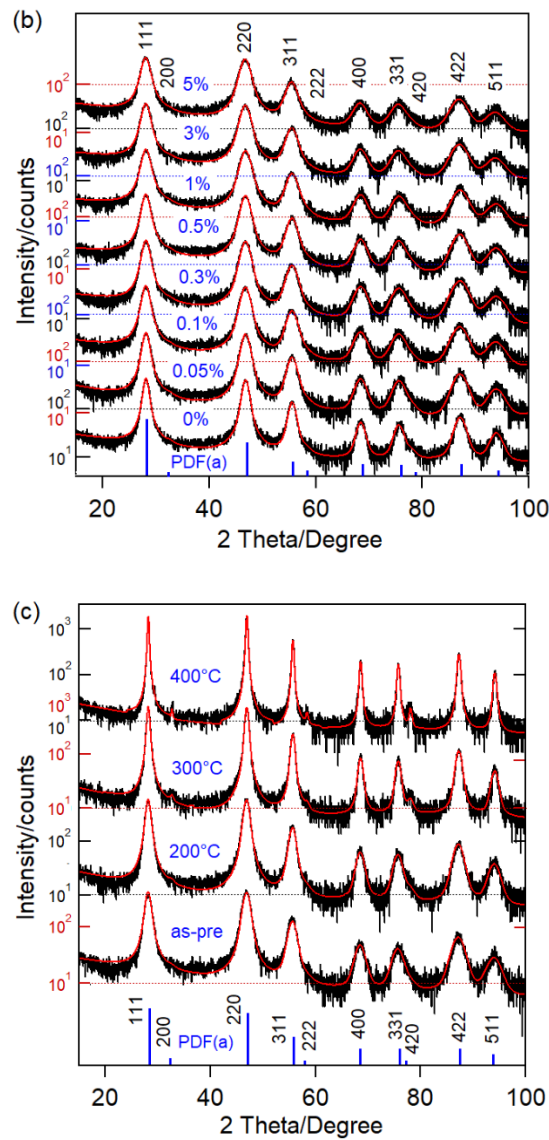


Figure 1. XRD patterns (semi-logarithmic plot) of (a) nanocrystalline $\text{CaF}_2\text{:}0.1\% \text{Sm}^{3+}$ prepared by ball milling for 1, 3, 5 and 8 h, (b) nanocrystalline $\text{CaF}_2\text{:}y\text{Sm}^{3+}$ with different concentration of Sm^{3+} ($0 \leq y \leq 5\%$) ball milled for 8 h, and (c) nanocrystalline $\text{CaF}_2\text{:}0.1\%\text{Sm}^{3+}$ as-prepared by ball milling for 8 h and subsequently annealed at 200, 300, and 400 °C. Experimental data and Rietveld refinements are shown as black and red lines, respectively. The standard data of cubic CaF_2 (PDF-1000043) is shown in blue. The green asterisks indicate impurity phases.

Table 1. Summary of XRD results obtained from Rietveld refinements. R_{wp} and R_{exp} are the weighted-profile R -factor and expected R -factor. G is the Goodness of fit (R_{wp}/R_{exp}).

Ball-milling time $\text{CaF}_2\text{:}0.1\% \text{Sm}^{3+}$					
time (h)	average crystallite size ± 1 (nm)	lattice parameter, a (Å)	Rietveld refinement		
			R_{wp} %	R_{exp} %	G
1	12	5.4754 ± 0.0012	18.9	14.5	1.30
3	11	5.4763 ± 0.0010	19.0	15.1	1.26
5	9	5.4823 ± 0.0012	19.4	14.9	1.30
8	8	5.4832 ± 0.0013	18.5	14.9	1.24
Concentration of Sm^{3+}					

CaF ₂ :ySm ³⁺ , 8 h ball-milling time					
y%	average crystallite size ± 1 (nm)	lattice parameter, a (Å)	Rietveld refinement		
			<i>R</i> _{wp} %	<i>R</i> _{exp} %	<i>G</i>
0	12	5.4824 ± 0.0011	15.9	13.9	1.14
0.05	11	5.4826 ± 0.0012	16.8	13.8	1.22
0.1	9	5.4832 ± 0.0013	18.5	14.9	1.24
0.3	9	5.4838 ± 0.0012	17.4	14.4	1.21
0.5	8	5.4844 ± 0.0011	17.8	15.2	1.17
1	8	5.4864 ± 0.0010	17.3	14.6	1.18
3	7	5.4880 ± 0.0014	17.1	14.5	1.18
5	6	5.4915 ± 0.0017	17.2	14.6	1.18
Annealing temperature CaF ₂ :0.1% Sm ³⁺ , 8 h ball-milling time					
temp. (°C)	average crystallite size ± 1 (nm)	lattice parameter, a (Å)	Rietveld refinement		
			<i>R</i> _{wp} %	<i>R</i> _{exp} %	<i>G</i>
as-pre	9	5.4774 ± 0.0011	20.9	15.0	1.39
200	12	5.4753 ± 0.0007	19.3	15.4	1.25
300	22	5.4701 ± 0.0004	18.7	15.3	1.22
400	45	5.4687 ± 0.0002	18.7	15.2	1.23

Typical TEM micrographs of CaF₂:0.1%Sm³⁺ prepared by ball milling are displayed in Figure 2. The observed crystallite/particle size distribution was in good agreement with the average crystallite sizes obtained from the Rietveld refinements. In particular, annealing the sample to 400 °C significantly increased the particle size. A micrograph of CaF₂:0.5%Sm³⁺ prepared by co-precipitation[20] with an average crystallite size of 46 ± 1 nm is shown in Figure 2e for comparison.

Photoluminescence spectra of nanocrystalline CaF₂:0.1%Sm³⁺ prepared by ball milling for 8 h before and after 360 Gy X-irradiation (Cu-Kα) are shown in Figure 3. Sm³⁺ emission lines centered at 566, 604, 645 and 704 nm (Figure 3a) correspond to ⁴G_{5/2} → ⁶H_J (*J* = 5/2, 7/2, 9/2, and 11/2) f-f transitions, respectively.[28–30] Sm³⁺ ⁴G_{5/2} → ⁶H_{5/2} and ⁶H_{7/2} transitions contain magnetic and electric dipole contributions that obey the selection rules Δ*J* = 0, ± 1, while the other two transitions ⁴G_{5/2} → ⁶H_{9/2} and ⁶H_{11/2} are purely electric dipole transitions (Δ*J* ≤ 6).[31] The symmetry of the local environment of the trivalent 4f ions can be identified by the relative intensity ratio of electric dipole to magnetic dipole transitions (*I*_R = ⁴G_{5/2} → ⁶H_{9/2} / ⁴G_{5/2} → ⁶H_{5/2}).[32] The present work indicated that most of the Sm³⁺ ions occupied the inversion symmetry sites of the CaF₂ host lattice since the *I*_R is < 1.[32–34] Note, however, that charge compensation will in principle lower the site symmetry.

Upon 360 Gy X-irradiation, the luminescence of Sm³⁺ decreased as is seen in Figure 3a accompanied by the rise of the electric dipole allowed Sm²⁺ 4f⁵5d (*T*_{1u}) → 4f⁶ ⁷F₁ (*T*_{1g}) transition at 708.2 nm with vibronic side bands (transverse optical phonon mode of CaF₂ due to the O_h⁵ group symmetry) (Figure 3b).[35–37] We stress here that no Sm²⁺ luminescence was observed before X-irradiation indicating that the Sm ions entered the CaF₂ host lattice in their +3 oxidation state. In contrast, Liu *et al.* reported the presence of Sm²⁺ emission lines in the absence of X-irradiation in nanocrystalline BaFCl:Sm³⁺ prepared by ball milling.[24]

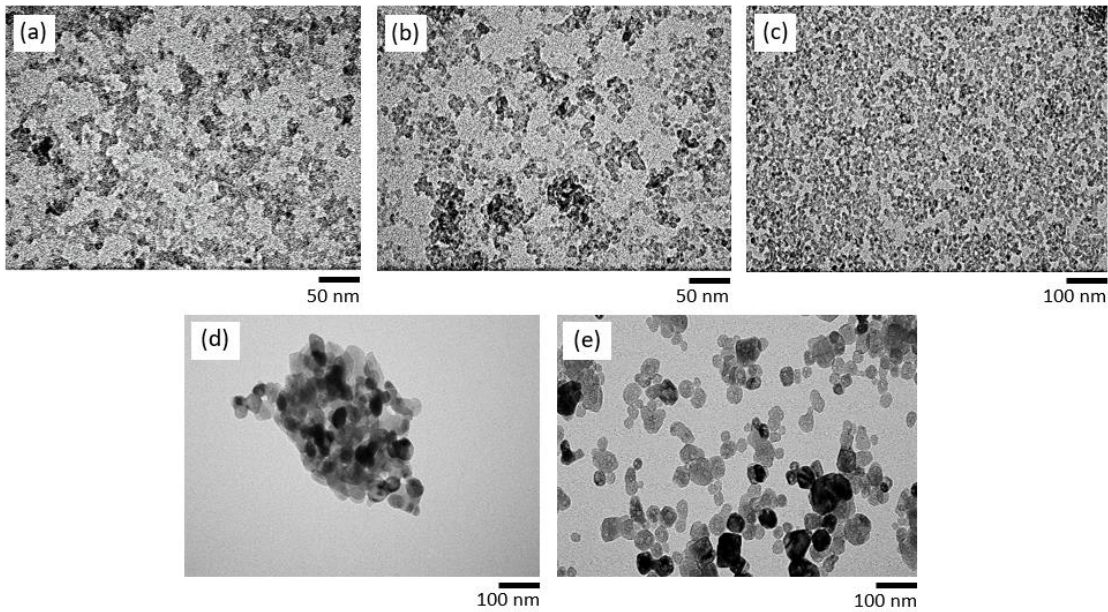


Figure 2. TEM micrographs of nanocrystalline $\text{CaF}_2:0.1\%\text{Sm}^{3+}$, ball milled for (a) 3 h and (b) 8 h, annealed at (c) 200 °C (d) 400 °C, and (e) nanocrystalline $\text{CaF}_2:0.5\%\text{Sm}^{3+}$ prepared by co-precipitation.

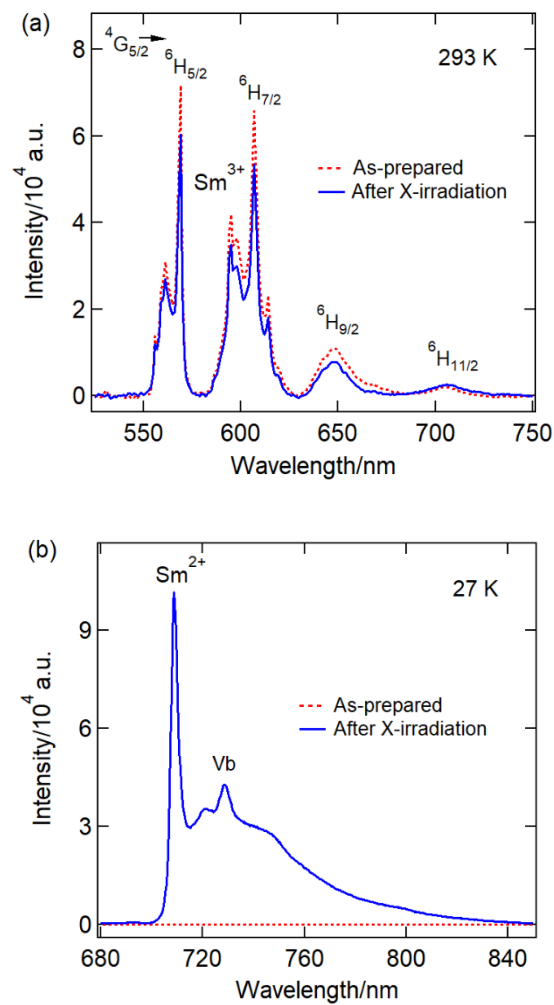


Figure 3. Photoluminescence spectra of nanocrystalline $\text{CaF}_2:0.1\% \text{Sm}^{3+}$ prepared by ball milling for 8 h before and after 360 Gy X-irradiation. (a) Region of Sm^{3+} luminescence at 293 K and (b) region of the $\text{Sm}^{2+} 4f^5 5d (T_{1u}) \rightarrow 4f^6 7F_1 (T_{1g})$ emission at 27 K.

In Figure 4 the photoluminescence spectra of nanocrystalline $\text{CaF}_2:0.1\% \text{Sm}^{3+}$ as a function of ball milling time are depicted. As follows from Figure 4a, the luminescence of Sm^{3+} increased with longer ball milling time. In contrast, the generation of Sm^{2+} upon X-irradiation gradually decreased with the ball milling time (Figure 4b). This may be due to a better embedding and charge compensation for longer ball milling times e.g. closer proximity of the charge compensators to the Sm^{3+} ions. It is also possible that with longer ball milling times, more defects are generated facilitating effective non-radiative deactivation paths for the Sm^{2+} .

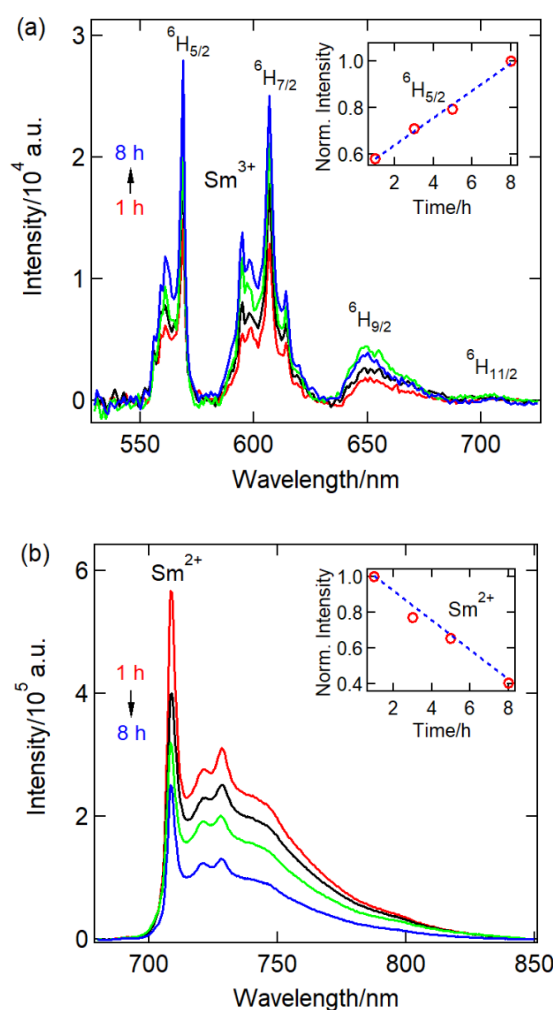


Figure 4. Photoluminescence spectra of nanocrystalline $\text{CaF}_2:0.1\% \text{Sm}^{3+}$ prepared by ball milling for 1, 3, 5 and 8 h. (a) Sm^{3+} region at 293 K of the as-prepared sample and (b) $\text{Sm}^{2+} 4f^5 5d (T_{1u}) \rightarrow 4f^6 7F_1 (T_{1g})$ region at 27 K after 135 Gy X-irradiation. The insets show corresponding integrated intensities as a function of ball milling time.

Photoluminescence spectra of nanocrystalline $\text{CaF}_2:y\text{Sm}^{3+}$ doped with different concentrations of Sm^{3+} ($0.05\% \leq y \leq 5\%$), and ball milled for 8 h are shown in Figure 5. As is seen in Figure 5a the intensity of Sm^{3+} luminescence lines of the as-prepared sample increased with the Sm^{3+} concentration for up to 1%, and then decreased with higher concentrations. Interestingly, the same trend was observed for the Sm^{2+} luminescence (upon 135 Gy X-irradiation) (Figure 5b). This concentration dependence is most likely due to quenching for concentrations higher than 1% induced by rapid

excitation energy transfer between the Sm ions that leads to non-radiative deactivation at trap sites.[38]

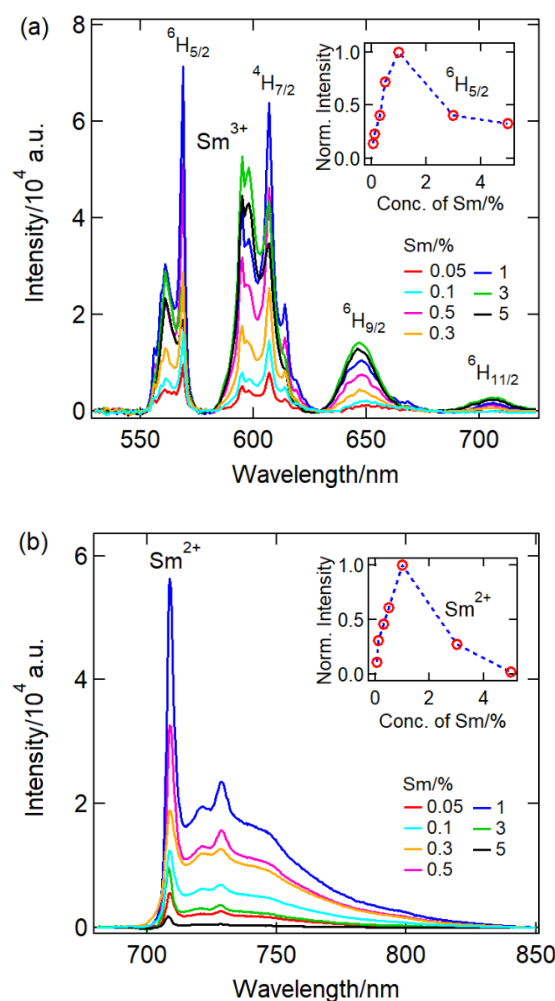


Figure 5. Photoluminescence spectra $\text{CaF}_2:y\text{Sm}^{3+}$ with $0.05\% \leq y \leq 5\%$ in the region of (a) Sm^{3+} at 293 K of the as-prepared sample and (b) $\text{Sm}^{2+} 4f^5 5d (T_{1u}) \rightarrow 4f^6 7F_1 (T_{1g})$ at 27 K upon 135 Gy X-irradiation. Integrated intensities of (a) $\text{Sm}^{3+} 4G_{5/2} \rightarrow 6H_{5/2}$ and (b) the Sm^{2+} emission band as a function of Sm concentration are shown in the insets.

In Figure 6, the effect of post-annealing for 1 h at 200, 300, and 400 °C on the luminescence of nanocrystalline $\text{CaF}_2:0.1\%\text{Sm}^{3+}$ (ball-milled for 8 h) is summarized. The figure shows that both the Sm^{3+} luminescence of the as-prepared sample (Figure 6a) and the Sm^{2+} luminescence of the X-irradiated samples (Figure 6b) became significantly stronger with increasing annealing temperature. The normalized photoluminescence intensity of the Sm^{3+} and Sm^{2+} emissions followed a $T^{2.4}$ and $T^{2.6}$ power law, respectively. An increase in photoluminescence intensity of the $\text{Sm}^{3+/2+}$ with increased temperature was previously observed by Liu *et al.* for $\text{BaFCl}:\text{Sm}^{3+}$. [39]

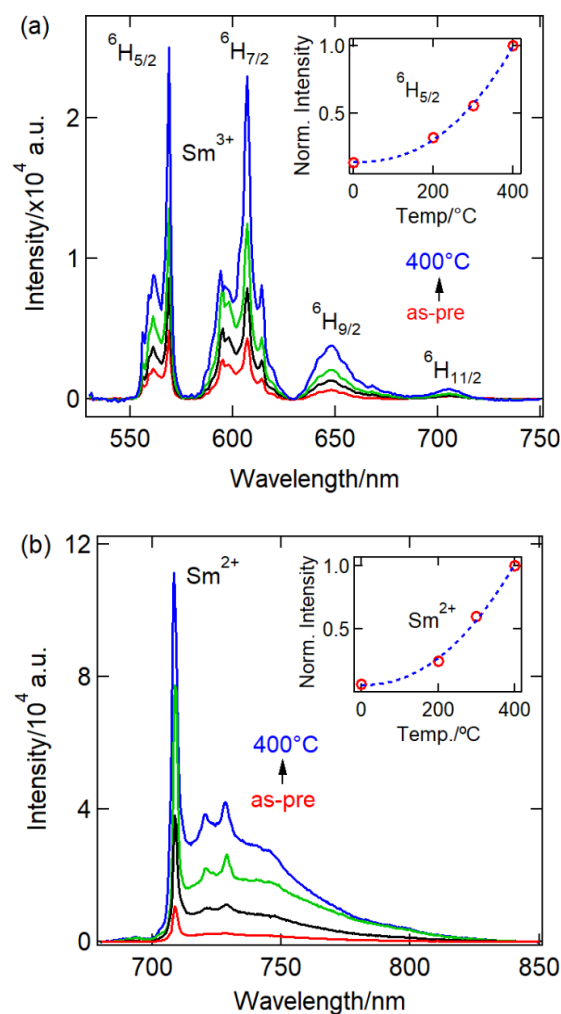


Figure 6. Photoluminescence spectra of $\text{CaF}_2:0.1\%\text{Sm}^{3+}$ annealed at 200, 300, and 400 °C for 1 h in air. (a) Sm^{3+} region of the as-prepared sample at 293 K, (b) Sm^{2+} region of the 135 Gy X-irradiated sample at 27 K. The inset of (a) and (b) show normalized intensities of Sm^{3+} and Sm^{2+} luminescence, respectively.

In Figure 7 a comparison is shown of the Sm^{2+} luminescence of X-irradiated (100 Gy) nanocrystalline $\text{CaF}_2:0.5\%\text{Sm}^{3+}$ prepared by co-precipitation (CPT) and as-prepared as well as annealed at 400 °C of $\text{CaF}_2:0.5\%\text{Sm}^{3+}$ prepared by 8 h of ball-milling (BM). As seen from the inset of the figure, the Sm^{2+} generation of BM $\text{CaF}_2:0.5\%\text{Sm}^{3+}$ showed a significantly increased by a factor 23 after annealed at 400 °C with crystallite size increased from 8 nm to 44 nm. In addition, both CPT $\text{CaF}_2:0.5\%\text{Sm}^{3+}$ and annealed BM $\text{CaF}_2:0.5\%\text{Sm}^{3+}$ had similar average crystallite sizes of 46 nm and 44 nm, respectively. However, in comparison with the CPT-sample, the Sm^{2+} luminescence intensity of the annealed BM-sample was lower by a factor of 3 after 100 Gy X-irradiation. This indicated a faster $\text{Sm}^{3+} \rightarrow \text{Sm}^{2+}$ conversion upon X-irradiation in the CPT sample compared to the BM samples. In the BM sample the trivalent Sm^{3+} may be more stabilized by a charge compensator due to the prolonged milling and annealing time, that enables ionic rearrangements of the lattice.[40]

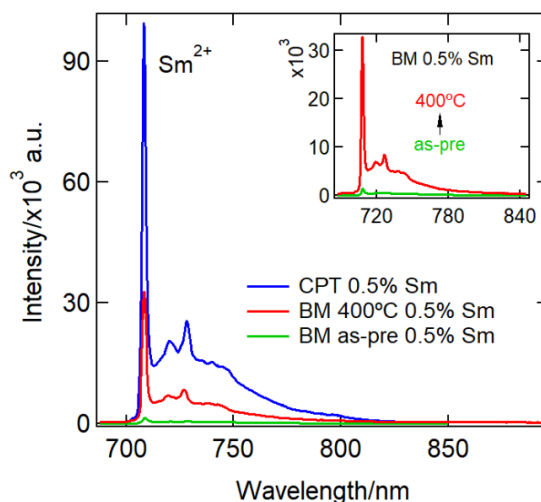


Figure 7. Comparison of photoluminescence spectra of nanocrystalline $\text{CaF}_2:0.5\%\text{Sm}^{3+}$ prepared by co-precipitation (CPT) and as-prepared as well as annealed at 400 °C of $\text{CaF}_2:0.5\%\text{Sm}^{3+}$ prepared by 8 h of ball-milling (BM). Inset shows 3x magnification of BM $\text{CaF}_2:0.5\%\text{Sm}^{3+}$.

4. Conclusions

We have reported a direct and facile mechanochemical preparation route for nanocrystalline $\text{CaF}_2:\text{Sm}^{3+}$ by ball milling $\text{Ca}(\text{OAc})$, $\text{Sm}(\text{OAc})_2$ and NH_4F at room temperature. The photoluminescence spectra of the as-prepared samples display the $\text{Sm}^{3+} {}^4\text{G}_J \rightarrow {}^6\text{H}_J$ luminescence lines whereas X-irradiation generates Sm^{2+} with its characteristic luminescence around 708 nm at low temperatures. A ball milling period of 3 to 4 h was found to result in the best single phase whereas shorter and longer ball milling resulted in some impurity phases. A longer ball milling period such as 8 h reduced the efficacy of Sm^{2+} generation by X-irradiation. This is likely due to the stabilization of the trivalent state by embedding the charge compensator in the vicinity of the Sm ion as well as more effective non-radiative deactivation by the introduction of more defects. Maximum luminescence was observed for the sample with a 1 mol% Sm^{3+} concentration, and at higher concentration quenching was observed. Interestingly, post-annealing substantially increases the X-ray induced Sm^{3+} to Sm^{2+} conversion. It is noted here that attempts to anneal at higher temperatures such as 1100°C (in air) generated extra phases in the XRD pattern with an associated change of the Sm^{3+} luminescence spectrum. In comparison with the co-precipitation (CPT)-sample, the Sm^{3+} ion in the ball milling-sample (BM) is much more stable. The present results demonstrated that the X-ray storage efficiency of nanocrystalline CaF_2 can be controlled in the preparation process by varying parameters such as ball milling time, annealing temperature and rare earth ion concentrations.

Author Contributions: Z.S.R.: Sample preparation, Investigation, Data curation, Formal Analysis, Writing - original draft. N.R.: TEM Analysis, Writing – Review & Editing. H.R.: Supervision, Conceptualization, Methodology, Writing – Review & Editing.

Funding:

Institutional Review Board Statement:

Informed Consent Statement:

Data Availability Statement:

Acknowledgments: We acknowledge the support of The University of New South Wales (UNSW) at the Australian Defence Force Academy for a University International Postgraduate Award. The authors thank Adelaide Microscopy as well as Dr Nobuyuki Kawashima of the Future Industries Institute at the University of South Australia for assistance with TEM imaging.

Conflicts of Interest: The authors declare no competing financial interests or personal relationships that could have been appeared to influence the work reported in this paper.

References

- Gerward, L.; Olsen, J. S.; Steenstrup, S.; Malinowski, M.; Åsbrink, S.; Waskowska, A. X-ray Diffraction Investigations of CaF₂ at High Pressure. *J. Appl. Crystallogr.* **1992**, *25*, 578-581.
- Hazen, R. M.; Finger, L. W. Calcium fluoride as an internal pressure standard in high-pressure crystallography. *J. Appl. Crystallogr.* **1981**, *14*, 234-236.
- Song, K. S.; Williams, R. T. Alkaline Earth Fluorides. In *Self-Trapped Excitons*; Song, K. S., Williams, R. T. Ed.; Springer Berlin Heidelberg. 1993; pp 96-122.
- Cheetham, A.; Fender, B.; Cooper, M. Defect structure of calcium fluoride containing excess anions I. Bragg scattering. *J. Phys. C: Solid State Phys.* **2001**, *4*, 3107.
- Ye, W.; Liu, X.; Qiyang, H.; Zhou, Z.; Hu, G. Co-precipitation synthesis and self-reduction of CaF₂:Eu²⁺ nanoparticles using different surfactants. *Mater. Res. Bull.* **2016**, *83*.
- Cantelar, E.; Sanz-García, J. A.; Sanz-Martín, A.; Muñoz Santiuste, J. E.; Cussó, F. Structural, photoluminescent properties and Judd-Ofelt analysis of Eu³⁺-activated CaF₂ nanocubes. *J. Alloys Compd.* **2020**, *813*, 152194.
- Pandurangappa, C.; Lakshminarasappa, B. N. Optical studies of samarium-doped fluoride nanoparticles. *Philos. Mag.* **2011**, *91*(35), 4486-4494.
- Ritter, B.; Krah, T.; Rurack, K.; Kemnitz, E. Nanoscale CaF₂ doped with Eu³⁺ and Tb³⁺ through fluorolytic sol-gel synthesis. *J. Mater. Chem. C.* **2014**, *2*(40), 8607-8613.
- Yuan, G.; Murai, S.; Tamura, S.; Tomita, K.; Tanaka, K. Enhancement of up- and downconversion photoluminescence from Yb³⁺, Er³⁺ co-doped CaF₂ nanoparticles deposited on two-dimensional plasmonic arrays. In *Proc. SPIE 11194, Plasmonics IV*, Hangzhou, China, 18 November 2019, Eds.; **2019**; Vol. 11194, pp 19.
- Nakhaei, O.; Shahtahmassebi, N.; Mahmood, R. Synthesis and Characterization of CaF₂ NPs with Co-precipitation and Hydrothermal Method. *J. Nanomed. Nanotechnol.* **2011**, *2*(5), 116.
- Quan, Z.; Yang, D.; Yang, P.; Zhang, X.; Lian, H.; Liu, X.; Lin, J. Uniform Colloidal Alkaline Earth Metal Fluoride Nanocrystals: Nonhydrolytic Synthesis and Luminescence Properties. *Inorg. Chem.* **2008**, *47*(20), 9509-9517.
- James, S.; Adams, C.; Bolm, C.; Braga, D.; Collier, P.; Friscic, T.; Grepioni, F.; Harris, K.; Hyett, G.; Jones, W., et al. Mechanochemistry: Opportunities for new and cleaner synthesis. *Chem. Soc. Rev.* **2011**, *41*, 413-447.
- Heise, M.; Scholz, G.; Düvel, A.; Heitjans, P.; Kemnitz, E. Mechanochemical synthesis, structure, and properties of solid solutions of alkaline earth metal fluorides: Ma_{1-x}Mb_xF₂ (M: Ca, Sr, Ba). *Solid State Sci.* **2016**, *60*, 65-74.
- Molaiyan, P.; Witter, R. Mechanochemical synthesis of solid-state electrolyte Sm_{1-x}CaxF_{3-x} for batteries and other electrochemical devices. *Mater. Lett.* **2019**, *244*, 22-26.
- Chowdhury, N.; Riesen, N.; Riesen, H. Yb³⁺ and Er³⁺ Codoped BaLiF₃ Nanocrystals for X-ray Dosimetry and Imaging by Upconversion Luminescence. *ACS Appl. Nano Mater.* **2021**, *4*(7), 6659-6667.
- Do, J.-L.; Frišić, T. Mechanochemistry: A Force of Synthesis. *ACS Cent. Sci.* **2017**, *3*(1), 13-19.
- Sadykov, V. A.; Mezentseva, N. V.; Bobrova, L. N.; Smorygo, O. L.; Ereemeev, N. F.; Fedorova, Y. E.; Bepalko, Y. N.; Skriabin, P. I.; Krasnov, A. V.; Lukashevich, A. I., et al. Chapter 12 - Advanced Materials for Solid Oxide Fuel Cells and Membrane Catalytic Reactors. In *Advanced Nanomaterials for Catalysis and Energy*; Sadykov, V. A. Ed.; Elsevier. 2019; pp 435-514.
- Düvel, A.; Wilkening, M.; Uecker, R.; Wegner, S.; Sepelak, V.; Heitjans, P. Mechanothesized nanocrystalline BaLiF₃: The impact of grain boundaries and structural disorder on ionic transport. *Phys. Chem. Chem. Phys.* **2010**, *12*, 11251-11262.
- Heise, M.; Scholz, G.; Krah, T.; Kemnitz, E. Luminescent properties of Eu³⁺ doped CaF₂, SrF₂, BaF₂ and PbF₂ powders prepared by high-energy ball milling. *Solid State Sci.* **2019**, *91*, 113-118.
- Rozaila, Z. S.; Riesen, N.; Riesen, H. Luminescence and photoionization of X-ray generated Sm²⁺ in coprecipitated CaF₂ nanocrystals. *Dalton Trans.* **2021**, *50*(44), 16205-16213.
- Crystallography Open Database. <http://www.crystallography.net/cod/index.php>. (accessed 2019-12-01).
- MAUD. <http://maud.radiographema.eu/>. (accessed 2019-12-02).
- Zhang, J.; Riesen, H. Photostimulated and persistent luminescence of samarium ions in BaFCl. *J. Lumin.* **2019**, *207*, 188-194.

24. Liu, Z.; Stevens-Kalceff, M. A.; Wang, X.; Riesen, H. Mechanochemical synthesis of nanocrystalline BaFCl:Sm³⁺ storage phosphor by ball milling. *Chem. Phys. Lett.* **2013**, *588*, 193-197.
25. Bensalah, A.; Mortier, M.; Patriarche, G.; Gredin, P.; Vivien, D. Synthesis and optical characterizations of undoped and rare-earth-doped CaF₂ nanoparticles. *J. Solid State Chem.* **2006**, *179*(8), 2636-2644.
26. Zhi, G.; Song, J.; Mei, B.; Weibing, Z. Synthesis and Characterization of Er³⁺ Doped CaF₂ Nanoparticles. *J. Alloys Compd.* **2011**, *509*, 9133-9137.
27. Shannon, R. D. Revised Effective Ionic Radii and Systematic Studies of Interatomic Distances in Halides and Chalcogenides. *Acta Crystallogr. A.* **1976**, *32*(5), 751-767.
28. Wells, J.-P. R. Laser Spectroscopy of Alkaline Earth Fluoride Crystals Doped With Trivalent Samarium and Europium Ions. *Ph.D. Thesis*, University of Canterbury, Christchurch, New Zeland, 1996.
29. Mikhail, P.; Ramseyer, K.; Frei, G.; Budde, F.; Hulliger, J. Bleaching of Sm²⁺ during photoluminescence and cathodoluminescence. *Opt. Commun.* **2001**, *188*, 111-117.
30. Rabbiner, N. Fluorescence of Sm³⁺ in CaF₂. *Phys. Rev. X.* **1963**, *130*, 502-506.
31. Bungala, C. J.; Kumar, M.; Gopal, K. Fluorescence properties and energy transfer mechanism of Sm³⁺ ion in lead telluroborate glasses. *Opt. Mater.* **2011**, *33*, 1643-1647.
32. Jamalaiah, B. C.; Rasool, S. N. Fluorescence properties of Sm³⁺ ions in yttrium aluminum borate phosphors for optical applications. *J. Mol. Struct.* **2015**, *1097*, 161-165.
33. Lakshminarayana, G.; Yang, R.; Mao, M.; Qiu, J.; Kityk, I. V. Photoluminescence of Sm³⁺, Dy³⁺, and Tm³⁺-doped transparent glass ceramics containing CaF₂ nanocrystals. *J. Non-Cryst. Solids.* **2009**, *355*(52), 2668-2673.
34. Qiao, Y.-P.; Chen, P. Luminescence, energy transfer, and color adjustment of CaO-CaF₂-Al₂O₃-B₂O₃-SiO₂ glass co-doped with CeO₂ and Sm₂O₃. *J. Non-Cryst. Solids.* **2021**, *552*, 120461.
35. Wood, D. L.; Kaiser, W. Absorption and Fluorescence of Sm²⁺ in CaF₂, SrF₂, and BaF₂. *Phys. Rev.* **1962**, *126*(6), 2079-2088.
36. Kelly-Gorham, M. R. K.; DeVetter, B. M.; Brauer, C. S.; Cannon, B. D.; Burton, S. D.; Bliss, M.; Johnson, T. J.; Myers, T. L. Complex refractive index measurements for BaF₂ and CaF₂ via single-angle infrared reflectance spectroscopy. *Opt. Mater.* **2017**, *72*, 743-748.
37. Kaiser, W.; Spitzer, W. G.; Kaiser, R. H.; Howarth, L. E. Infrared properties of CaF₂, SrF₂, and BaF₂. *Phys. Rev.* **1962**, *127*(6), 1950-1954.
38. Qiao, Y.-P. Influence of Sm₂O₃ and CaF₂ Concentration on the Enhancement of Luminescence and Red Colour in Borosilicate Glass. *Trans. Indian Ceram. Soc.* **2021**, *80*(3), 208-215.
39. Liu, Z. Q.; Stevens-Kalceff, M. A.; Riesen, H. Effects of Postannealing on the Photoluminescence Properties of Coprecipitated Nanocrystalline BaFCl:Sm³⁺. *J. Phys. Chem. A.* **2013**, *117*(9), 1930-1934.
40. Stevens-Kalceff, M. A.; Liu, Z.; Riesen, H. Cathodoluminescence Microanalysis of Irradiated Microcrystalline and Nanocrystalline Samarium Doped BaFCl. *Microsc. Microanal.* **2012**, *18*(6), 1229-1238.

Disclaimer/Publisher's Note: The statements, opinions and data contained in all publications are solely those of the individual author(s) and contributor(s) and not of MDPI and/or the editor(s). MDPI and/or the editor(s) disclaim responsibility for any injury to people or property resulting from any ideas, methods, instructions or products referred to in the content.